Dalton Transactions

ROYAL SOCIETY OF CHEMISTRY

PAPER

View Article Online
View Journal | View Issue

Cite this: *Dalton Trans.*, 2025, **54**, 16037

Photophysical studies on *meta*- and *para*-carboranes containing 1-naphthyl groups

Rachel A. Harder,[a] Thomas D. McGurrell,[a] J. A. Hugh MacBride,[a] Lena Böhling,[b] Andreas Brockhinke,[b] Dmitry S. Yufit[a] and Mark A. Fox *[a]

Received 10th September 2025,
Accepted 7th October 2025

DOI: 10.1039/d5dt02179k

rsc.li/dalton

Four new carboranes, *C*-(1-naphthyl)-*meta*-, *C*,*C*′-bis(1-naphthyl)-*meta*-, *C*-(1-naphthyl)-*para*- and *C*,*C*′-bis(1-naphthyl)-*para*-carborane, reveal high-energy emissions at 332–343 nm with quantum yields of 21–38% and long lifetimes of 26–31 ns in degassed cyclohexane solutions. The experimental absorption and emission spectra of the mononaphthyl carboranes are successfully simulated by hybrid DFT vibronic calculations. The computed lowest energy excited state (S_1) geometries contain non-planar naphthyl groups due to shorter carborane C–aromatic C bonds and steric effects between the bulky naphthyl and carboranyl units. The high energy emissions are also reproduced in polymethylmethacrylate (PMMA) films and as solids. The lower energy emissions in 99 : 1 water : THF suspensions for these four compounds at 385–421 nm show quantum yields of 50–64% and long lifetimes of 28–40 ns. The findings indicate that *meta*- and *para*-carborane derivatives can generate different solid-state emissions as reported elsewhere for the intensively researched *ortho*-carborane analogues.

Introduction

Organic luminophores containing icosahedral *ortho*-carborane (1,2-$C_2B_{10}H_{12}$) have been intensively studied in the last decade partly due to the ability of the cluster to take part in the charge transfer (CT) emissions as the acceptor in some dyads.[1–3] Dual emissions are observed in some derivatives where local emission (LE) at the organic fluorophore and CT emission involving both the organic moiety and the carborane cluster are simultaneously observed.[1–7]

Solid-state emissions of these carborane fluorophores have been demonstrated to vary considerably depending on the solid morphologies.[8–11] While some emissions observed can be attributed to charge transfer involving the carborane cluster,[12] local, solid state intermolecular interactions and specific conformers were also inferred to be responsible for emissions present.[13] Aggregation-induced emissions (AIEs) in these *ortho*-carborane fluorophores are usually reported from solid suspensions in 99 : 1 water : tetrahydrofuran solutions with high quantum yields.[14,15]

Organic fluorophores involving *meta*- and *para*-carboranes (1,7- and 1,12-$C_2B_{10}H_{12}$ respectively) are less studied as these clusters do not generally participate in emissions with no flexible cluster C–C bond present to readily accept an electron.[5]

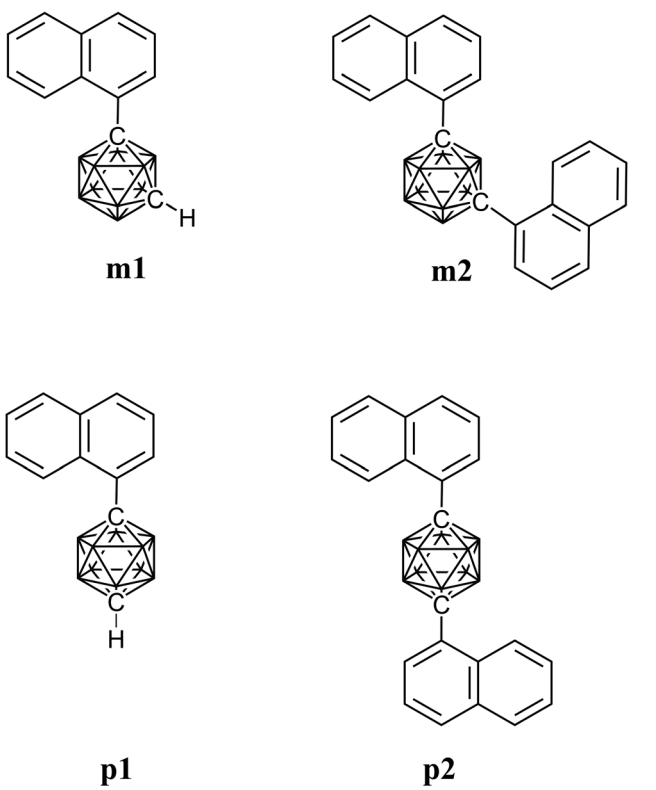

Fig. 1 Compounds investigated in this study. Each naked vertex represents BH.

[a]*Department of Chemistry, Durham University, Lower Mountjoy, Stockton Road, Durham DH1 3LE, UK. E-mail: m.a.fox@durham.ac.uk*
[b]*Department of Chemistry, Bielefeld University, Universitätstraße 25, 33615 Bielefeld, Germany*

They are usually considered as spectators with little/no active role in the photophysics where the organic luminophore unit is present. Nevertheless, these clusters were recently described as active conduits between donor and acceptor units.[16]

Organic luminophores with fused aromatic rings (naphthalene,[17–23] anthracene,[19,24–33] phenanthracene,[34–38] pyrene,[39–43] fluoranthene[44] and chrysene[45]) at the cage carbons of *ortho*-carborane clusters have been researched intensively and revealed many intriguing emissions. For example, *C*,*C*′-bis(1-naphthyl)-*ortho*-carborane gave three distinct emissions (LE, CT and intramolecular excimer).[17] By contrast, the field of *meta*- and *para*-carborane analogues containing fused organic rings attached to the cluster carbons are under-developed with only three examples known.[26,28] Here, the photophysics of four *meta*- and *para*-carboranes with 1-naphthyl groups attached at one or both carborane carbon(s) are described with hybrid density functional theory (DFT) data successfully simulating their absorption and emission spectra (Fig. 1).

Results and discussion

C-Naphthylcarboranes (**m1**, **m2**, **p1**, **p2**, Fig. 1) were synthesised in moderate yields (16–59%) from the corresponding parent carborane and iodonaphthalene using the well-established coupling method for *C*-aryl-*meta*- and *para*-carboranes (Fig. 2).[46,47] Replacing iodonaphthalene with bromonaphthalene, using this method also gave similar yields of the desired products, **m1** and **m2**, from *meta*-carborane. Unlike the other three soluble carboranes, dinaphthyl-*para*-carborane is partly soluble or insoluble in many organic solvents.

The compounds were characterised by multinuclear NMR, infrared (IR) and mass spectra (Fig. S1–S28). Sextet peaks corresponding to the carborane C–H proton were observed in the $^{1}H\{^{11}B\}$ NMR spectra of the mononaphthyl products arising from $^{3}J_{HH}$ couplings with the five neighbouring B–H protons.[48] The ^{13}C NMR peaks of the naphthyl group in all compounds were assigned with the aid of 2D COSY and correlation spectra.[49]

Single crystal X-ray diffraction studies on these naphthalenes confirmed their identities with the expected planar naphthyl groups occupying orientations with negligible steric repulsions between the naphthyl group and the cluster.[17] These observations differ from the reported[28] *C*-anthracenyl *meta*- and *para*-carboranes where the anthracenyl groups are non-planar to accommodate the steric repulsions between the fused rings and the cluster. The carborane cluster can be disordered in crystals as both BH and CH vertices can interchange due to similar sizes.[50] The crystal structures for the mononaphthyl carboranes contain ordered clusters due to the carborane C–H···π(aryl) interactions present (Fig. 3 and Table 1).[51]

The intermolecular interactions in the crystal structures of the dinaphthyl carboranes are aryl C–H···π(ring) interactions where one unique intermolecular interaction in **m2** is substantially stronger than the other interactions in the crystal structures.(Fig. 4 and Table 1) This strong interaction is reflected by the shorter H···ring distance of 2.465 Å and the favourable directing C–H···ring angle of 175.9°.

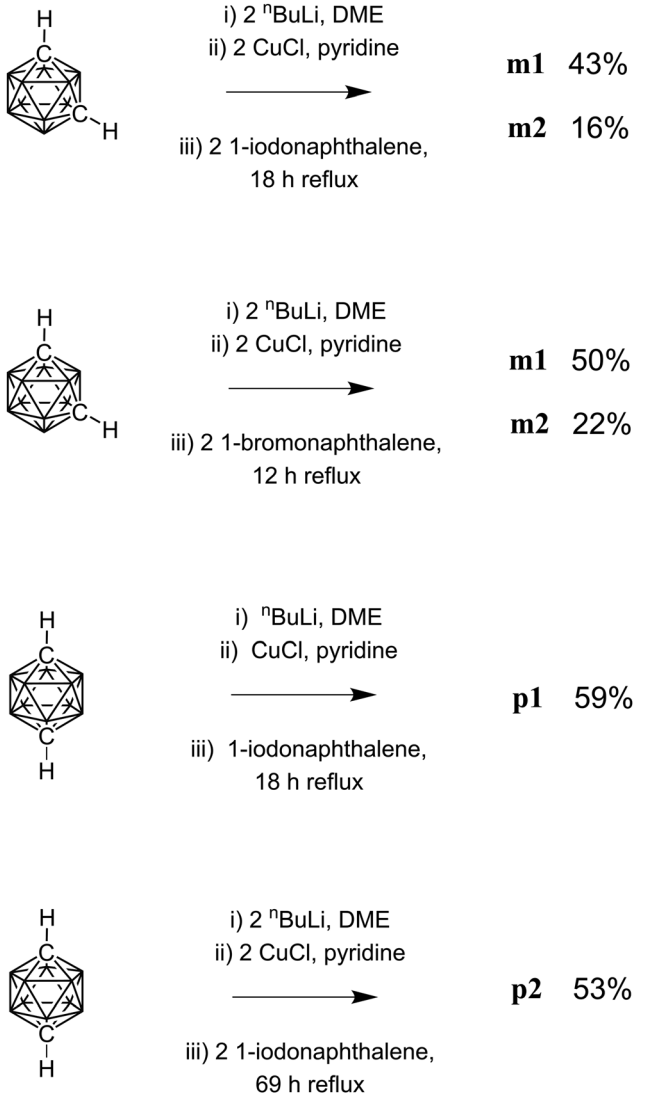

Fig. 2 Scheme summarising the synthetic routes to *C*-naphthylcarboranes.

Photophysics

Solution-state absorption spectra of the carboranes showed absorption maxima at 290 nm with vibronic structure indicating local absorption at the naphthyl groups[52] (Fig. 5a, S29–S32 and Table S1). A strong higher energy broad band at 230 nm is also observed in cyclohexane for each compound and is likely to also arise from naphthyl group absorption since carborane absorption bands are extremely weak in this region.[53]

Solution state emissions for all compounds had high energy maxima at 332–341 nm with vibronic structures observed in cyclohexane (CHX) which become less well defined in the more polar solvent dichloromethane (DCM,

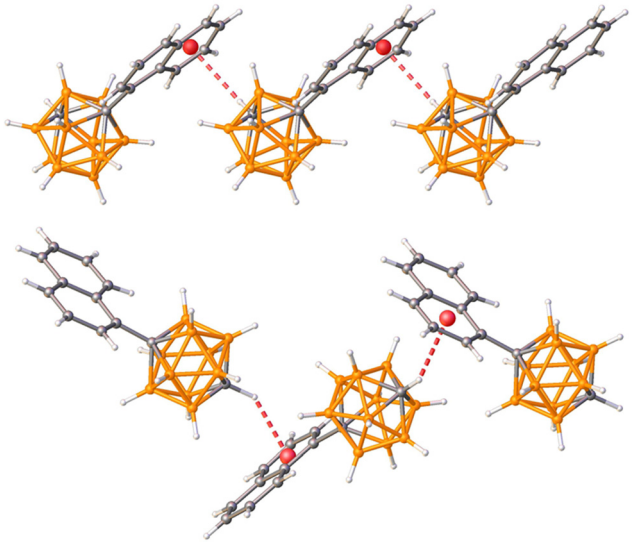

Fig. 3 Carboranyl C–H···.π(ring) intermolecular interactions in crystals of *C*-mononaphthyl-carboranes (**m1** top and **p1** bottom).

Table 1 Intermolecular interaction parameters, values in bold are interactions with the C5–10 ring. Hydrogens are normalised (C–H bond length = 1.089 Å). Cent = centroid of aromatic ring

	H···Cent (Å)	C ···Cent (Å)	C–H···Cent angle (°)
m1	**2.687**	**3.562**	**137.0**
m2	**2.465**, 2.538	**3.552**, 3.520	**175.9**, 149.5
p1	2.668, 2.620	3.625, 3.591	148.1, 146.3
p2	2.535	3.478	144.3

Fig. 5a, S29–S32 and Table 2). These ultraviolet emissions arise from local excitation of the naphthyl groups. Naphthyl derivatives have long been known to be sensitive to oxygen quenching[52] and are observed here for cyclohexane solutions where quantum yields and lifetimes in deaerated : aerated ratios of roughly 2 : 1 with a strong correlation between quantum yields and lifetimes.[54] Emissions of the carboranes in dichloromethane solutions remain unchanged when aerated or deaerated (Fig. S33). Oxygen-quenching also takes place in the emissions of toluene, tetrahydrofuran (THF), acetonitrile (MeCN) and dimethylformamide (DMF) solutions for dinaphthyl-*meta*-carborane (Fig. S36 and Table S3) with lower deaerated : aerated ratios.

Quantum yields and lifetimes (τ) of these four carboranes measured in deaerated cyclohexane solutions are in the ranges of 22–38% (Φ^F = 0.22–0.38) and 27–32 ns respectively (Table 2 and Fig. S35). These lifetimes are longer than the long lifetime of 22.5 ns reported for *C*-(1-pyrenyl)-*ortho*-carborane.[7] When these cyclohexane solutions are aerated, the yields drop to 14–16% and lifetimes shortened to 11–15 ns. In dichloromethane solutions, the QY range drops further to 8–12% and the lifetimes are shorter at 7–9 ns. The radiative rates k_r for the cyclohexane and dichloromethane solutions of the carboranes are in the narrow region of 0.75–1.64 s^{-1}. This narrow range reflects virtually identical high-energy emissions from the naphthyl groups (LE) in these carboranes.

Solid state photophysical data on the carboranes were also explored in the form of polymethylmethacrylate (PMMA) films, suspensions from rapid precipitation of tetrahydrofuran (THF) solution with water (1 : 99 THF : water ratio) and as evaporated solid films (Fig. 5b, S34 and Table 3). The PMMA films would contain isolated solid molecules – likely in different conformers – ruling out intermolecular interactions responsible for these solid-state emissions. The solid suspensions would logically form aggregates as amorphous solids where intermolecular interactions and multiple conformers are expected to be present and may contribute to the emissions observed. The slow evaporation of dichloromethane solutions onto quartz plates would be expected to result in microcrystalline solids and the emissions shown may arise from the specific monomer conformer or from excimers due to intermolecular interactions present in the crystal form.

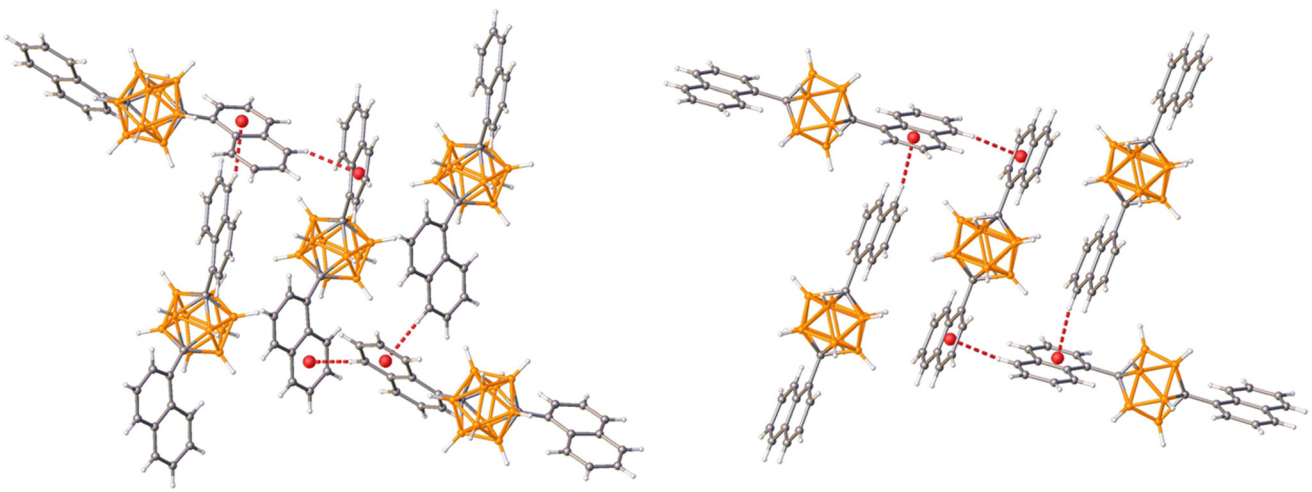

Fig. 4 Aromatic C–H···.π(ring) intermolecular interactions in crystals of *C*,*C*′-dinaphthyl-carboranes (**m2** left and **p2** right).

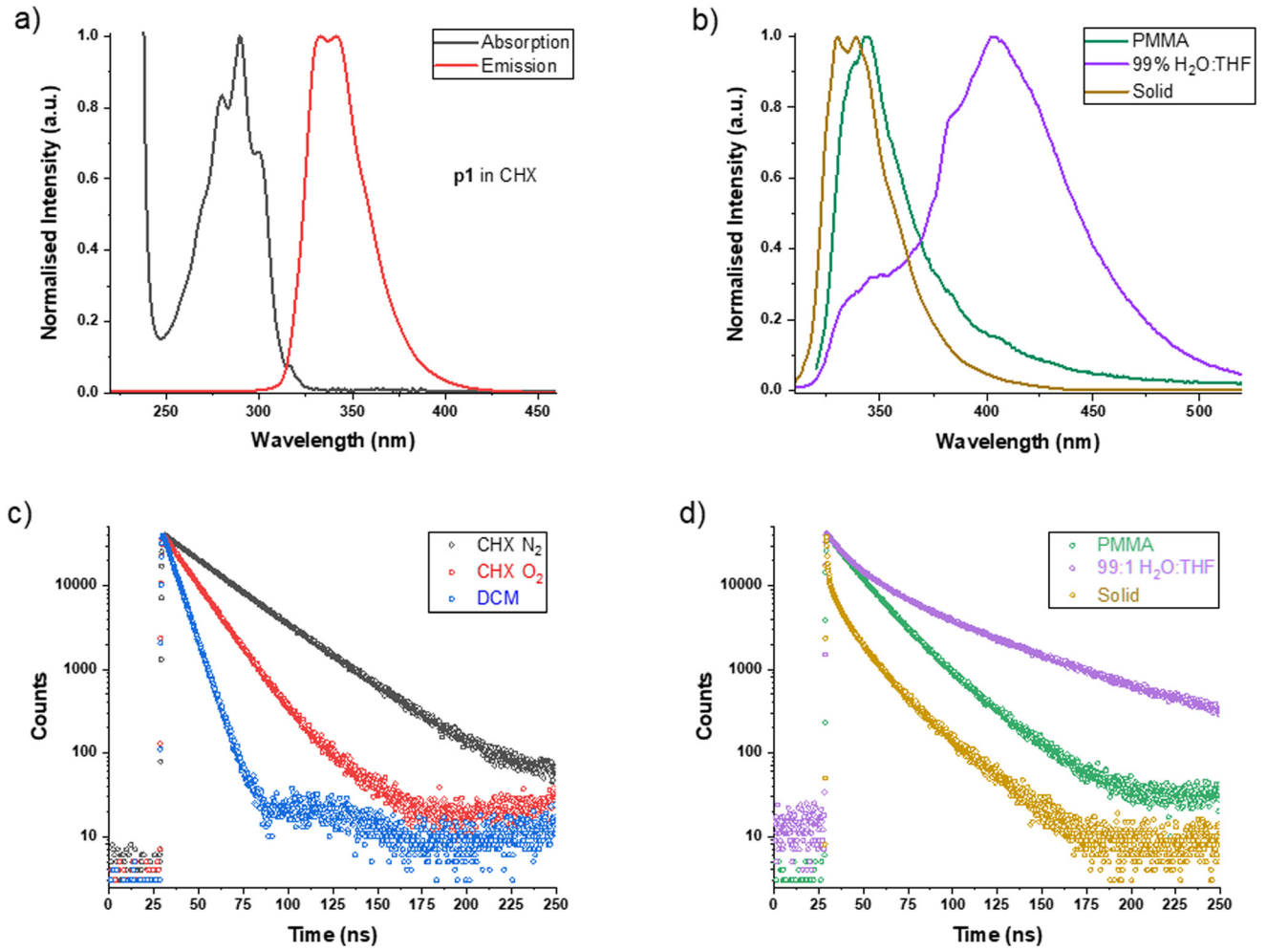

Fig. 5 Photophysical data for *C*-naphthyl-*para*-carborane **p1**. (a) Absorption and emission spectra in cyclohexane (CHX). (b) Solid state emission spectra. (c) Solution state lifetimes. (d) Solid state lifetimes.

The high energy emissions from PMMA films with minima 343–345 nm for all four compounds indicate similar photophysical processes to those found in solutions. The broad and lower energy emissions from the solid carborane suspensions of 1 : 99 THF : water mixtures in all compounds with maxima at 374–421 nm suggest that several conformers combined with intermolecular interactions in the form of either naphthyl–naphthyl or naphthyl–cluster or both result in excimers to give these ill-defined emissions. The high energy shoulders at 320–350 nm in the emission spectra of these 1 : 99 THF : water mixtures indicate that monomers – and crystalline forms in the case of **m1**, **p1** and **p2** – are also present in the solid state particles. Unlike the pure crystalline forms, the solid particle morphologies in these THF : water mixtures are not determined but expected to contain irregular powder and crystalline forms.

More structured high energy emissions at 330–343 nm were observed for the solid films except for the dinaphthyl-*meta*-carborane **m2** at 385 nm. Based on the crystal structures determined here, it is concluded that the stronger intermolecular interactions present in **m2** with short H···ring distance of 2.465 Å and the favourable directing C–H···ring angle of 175.9° cause the red shifting of the emission maximum with respect to its solution state and PMMA emissions. This emission is likely to arise from intermolecular excimers with these short interactions between naphthyl groups in the crystalline state. Such excimers are not present in the crystalline forms of **m1**, **p1** and **p2** presumably as the intermolecular interactions in the crystal forms are too weak to give excimers thus only LE (monomer) emissions are present for **m1**, **p1** and **p2**. The crystalline form of **m2** may also exist in the 1 : 99 THF : water mixture of **m2** along with excimers of different conformations.

The quantum yields and lifetimes in these three different solid forms were measured. The solid suspensions contain the highest quantum yields and average lifetimes, the solid films the lowest while the PMMA films are in between (Fig. 5d, S37, Tables 3 and S2). Unlike the lifetime measurements in solutions with exponential decay profiles, non-exponential decays are present in these solids.

The emissions are enhanced in the solid suspensions with quantum yields of 50–64% and attributed to aggregation

Table 2 Solution state emission data

	Emission maxima[a] (nm)	Quantum yield[b] (QY, %)	Lifetime[c] (τ, ns)	Radiative rate[d] (k_r, 10^7 s^{-1})	Non-radiative rate[e] (k_{nr}, 10^7 s^{-1})
m1					
Cyclohexane N_2	332, 340	35.5	31.8	1.12	2.03
Cyclohexane O_2	332, 340	14.2	13.8	1.03	6.22
N_2 : O_2 ratio[f]		*2.5*	*2.3*		
Dichloromethane	338	9.6	7.4	1.30	12.2
m2					
Cyclohexane N_2	333, 340	38.3	30.4	1.26	2.03
Cyclohexane O_2	333, 340	15.2	14.3	1.06	5.93
Ratio		*2.5*	*2.1*		
Dichloromethane	339	11.5	7.0	1.64	12.7
p1					
Cyclohexane N_2	333, 341	21.8	29.1	0.749	2.69
Cyclohexane O_2	333, 341	14.4	15.0	0.960	5.71
Ratio		*1.5*	*1.9*		
Dichloromethane	340	8.0	9.1	0.879	10.1
p2					
Cyclohexane N_2	332, 342	32.0	26.9	1.19	2.53
Cyclohexane O_2	332, 342	16.2	10.5	1.54	7.98
Ratio		*2.0*	*2.6*		
Dichloromethane	333, 340	10.7	7.1	1.51	12.6
Naphthalene					
Cyclohexane N_2	322, 334	29.4	105.3	0.28	0.67
Cyclohexane O_2	322, 334	3.9	18.2	0.21	5.28
Ratio		*3.6*	*5.8*		
Dichloromethane	322, 334	1.9	8.9	0.21	11.0

[a] Excited at 300 nm. [b] Measured with integrating sphere, Φ^F = QY/100. [c] Excited at 317 nm. Exponential decay fitting. [d] $k_r = \Phi^F/\tau$ in s^{-1}. [e] $k_{nr} = 1 - \Phi^F/\tau$ in s^{-1}. [f] Ratio of deaerated : aerated values; $\Phi^F(N_2)/\Phi^F(O_2)$ and $\tau(N_2)/\tau(O_2)$.

Table 3 Solid state emission data

	Emission maxima[a] (nm)	Quantum yield[b] (QY, %)	Average lifetime[c] (τ, ns)	Radiative rate[d] (k_r, 10^7 s^{-1})	Non-radiative rate[e] (k_{nr}, 10^7 s^{-1})	CIE 1931 coordinates
m1						
PMMA film	343	26.0	13.8	1.88	5.36	0.172, 0.005
99 : 1 H_2O : THF	407	56.7	31.1	1.82	1.39	0.157, 0.028
Solid film	333, 343	1.0	0.6	1.67	165	0.174, 0.005
m2						
PMMA film	345	29.6	17.6	1.68	4.00	0.170, 0.006
99 : 1 H_2O : THF	374	64.2	34.0	1.89	1.05	0.163, 0.094
Solid film	385	22.8	4.7	4.85	16.4	0.173, 0.042
p1						
PMMA film	343	28.3	17.2	1.65	4.17	0.171, 0.006
99 : 1 H_2O : THF	402	49.5	39.9	1.24	1.27	0.159, 0.021
Solid film	330, 339	13.4	2.2	6.09	39.4	0.173, 0.006
p2						
PMMA film	344	18.6	7.0	2.66	11.6	0.172, 0.005
99 : 1 H_2O : THF	421	52.9	28.7	1.84	1.64	0.154, 0.068
Solid film	337, 343	20.5	7.5	2.73	10.6	0.173, 0.006
Naphthalene						
PMMA film	322, 335	46.2	67.6	0.68	0.80	0.175, 0.005
99 : 1 H_2O : THF	334	29.7	35.5	0.84	1.98	0.174, 0.005
Solid film	333, 336	70.3	71.9	0.98	0.41	0.174, 0.005

[a] Excited at 300 nm. [b] Measured with integrating sphere, Φ^F = QY/100. [c] Excited at 317 nm. Non-exponential decay fitting. [d] $k_r = \Phi^F/\tau$ in s^{-1}. [e] $k_{nr} = 1 - \Phi^F/\tau$ in s^{-1}.

induced emissions (AIE) reported in many studies elsewhere for *ortho*-carborane derivatives.[8–11] It is noted here that the desired carborane AIE properties are not exclusive to *ortho*-carboranes. The observed fluorescence lifetimes are also remarkably long with values in the region of 29–40 ns. These lifetimes are longer than the solid suspension (1 : 99 THF : water) of the *ortho*-carborane chrysene reported at 23 ns.[45]

The quantum yields 18.6–29.6% and lifetimes 7.0–17.6 ns for the PMMA films in all four carboranes are slightly different to the corresponding values found in solutions. These results

suggest that free naphthyl-carborane rotations taking place in solutions and varied but static conformers present in PMMA films do not change the observed emission processes. This contrasts with many reports of *ortho*-carborane derivatives where non-radiative processes dominate in solutions but not in solid states.

A monoaryl-*ortho*-carborane can have three distinct excited states where the cluster does not take part in the organic local emission (LE), the elastic cluster C–C bond lengthens to act as an acceptor in a charge transfer (CT) emission and the cluster C–C bond lengthens further to a third excited state where a non-radiative relaxed process is expected.[7] The non-radiative processes for *ortho*-carborane derivatives in solutions may in part be from the third carborane excited states accessed in solutions. These non-radiative pathways are hampered in the solid states due to the rigid geometry constraints of the solid states. The reported CT and non-radiative excited states with the *ortho*-carborane cluster do not apply to *meta- and para*-carborane clusters as there are no intracluster carborane C–carborane C bonds in the latter clusters.

The crystalline solid films of the naphthyl carboranes generally have shorter lifetimes and lower quantum yields than the corresponding PMMA films and 1 : 99 THF : water solid suspensions. Clearly, the specific conformers in the crystals are not ideal for high emission efficiencies especially for **m1** where a QY of only 1% was observed. The similar QY and lifetime values found for the PMMA film and crystalline solid of **p2** indicate that mixed conformers in PMMA have little effect on the emissions for this compound.

The radiative rates k_r for the PMMA films, solid suspensions and solid films of the carboranes are 1.7–2.7, 1.2–1.9 and 1.7–6.1 × 10^{-7} s^{-1} respectively. Despite the different emission types and maxima, the PMMA films and solid suspensions have similar radiative rates. However, the radiative rates for the solid films are varied and appear to subtly depend on the specific conformer in each crystal structure.

The CIE 1931 coordinates of 0.17, 0.01 reflect the UV-violet high energy emissions in solutions and in PMMA films when excited at 300 nm. The solid suspensions contain visible deep blue emissions with coordinates at 0.15–0.16, 0.03–0.09. The solid films show visible violet emissions as the bands trail to 460 nm (Fig. S38).

Low temperature emission spectra were also measured for all carboranes in cyclohexane and dichloromethane at 77 K. Highly structured, intense emissions with emission maxima in the region of 322–342 nm at 2 μM concentrations were observed and assigned as vibronic LE (monomer) emissions (Fig. S39 and Table S4). Broad low energy emissions were present along with the high energy vibronic bands at higher concentrations of 20 μM. These broad low energy emissions are from excimers. The low temperature broad emissions in the region between 350 and 500 nm in cyclohexane resemble the emissions from 1 : 99 THF : water mixtures for the carboranes. Naphthalene and its derivatives have long been known to form excimers at higher concentrations and at lower temperatures.[55]

It is instructive here to compare the photophysics of naphthylcarboranes with naphthalene itself to assess the roles of the carboranyl groups on the photophysical aspects. Data measured here for naphthalene are listed in Tables 2 and 3 for direct comparison with the naphthylcarboranes (Fig. S40–S42 and Table S5). The carboranyl units have little effect on the emission maxima with red shifts in the region of 940 cm^{-1} (0.11 eV) in energies and similar quantum yields with respect to the parent naphthalene in solutions. The lifetimes are decreased and radiative rates increased when the carborane is present compared to the parent naphthalene.

Table 4 Aromatic deformation parameters for 1-naphthylcarboranes

	Cage C–C bond length (Å)	Inter-ring plane angle (°)	α (°)	β (°)
X-ray				
m1	1.524	5.03	4.63	2.18
m2	1.522	3.46, 5.08	2.99, 4.08	2.48, 1.67
p1	1.530	1.52, 0.70	1.34, 1.38	2.22, 1.78
p2	1.542	1.76	0.73	1.85
Computed S_0				
m1	1.526	0.76	0.87	1.53
m2	1.526	1.86	1.99	1.54
p1	1.529	0.00	0.00	1.67
p2	1.527	0.00	0.00	1.56
Computed S_1				
m1	1.494	7.81	12.98	4.91
m2	1.493, 1.526	8.68, 1.76	14.08, 1.87	4.93, 1.46
p1	1.494	8.63	14.00	5.19
p2	1.491, 1.526	8.57, 0.00	13.83, 0.00	4.12, 1.70

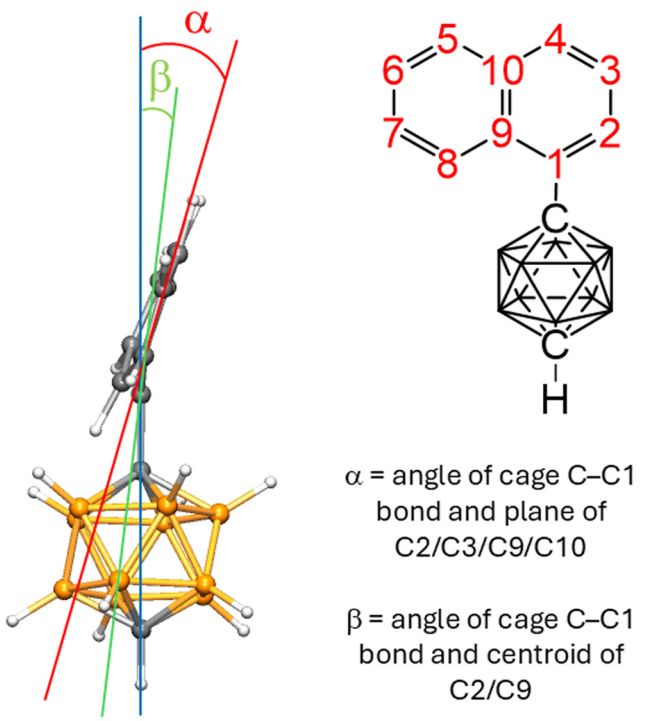

Fig. 6 Definition of the angles, α and β, as a measure of non-planarity in carboranes with the numbering scheme for the naphthyl group. Each naked vertex represents BH.

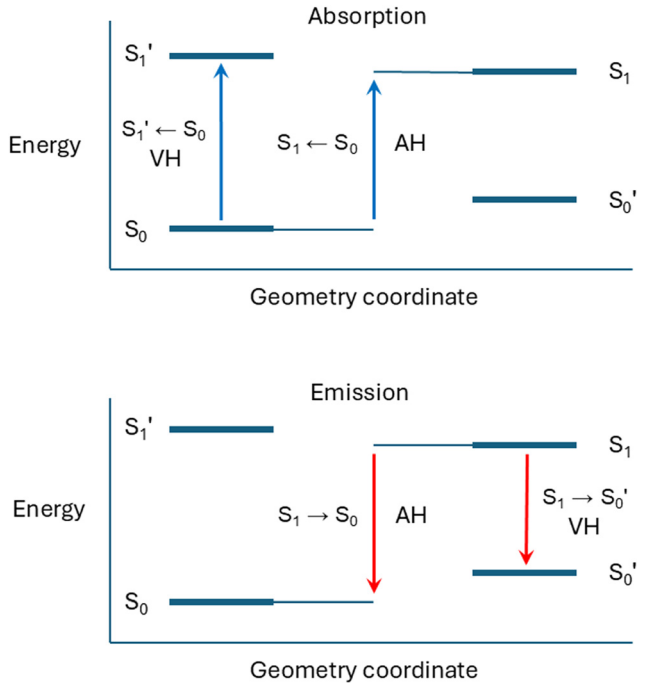

Fig. 7 Vertical (VH) and adiabatic Hessian (AH) calculations used in predicting absorption and emission energies.

The differences between naphthalene and the naphthylcarboranes are more marked in the solid-state emission data as excimer emissions are not present for the parent naphthalene under these conditions. With respect to high energy emissions only, the carborane units significantly reduce the quantum yields and emission lifetimes and increase the radiation rates compared to pure naphthalene. When considering 1 : 99 THF : water mixtures, the high energy LE emission of naphthalene has a quantum yield of 30% which is lower than the 50–64% yields for the low energy excimer emissions of the naphthylcarboranes.

Computations

Optimised geometries for all four at S_0 ground states were explored with the range-corrected DFT hybrid CAM-B3LYP functional here. Mononaphthyl-*para*-carborane has only one minimum located due to its high symmetry and a planar naphthyl group thus the model of choice for detailed computations here. There are 3 minima located for mononaphthyl-*meta*-carborane and for dinaphthyl-*para*-carborane whereas 7 minima were identified for dinaphthyl-*meta*-carborane. Simulated and observed infrared spectra were in excellent agreement when the energy scaling factor[56] of 0.945 was applied (Fig. S21–S24). Optimised and X-ray determined geometries were also in very good agreement with all cluster C–naphthyl C bond lengths in the 1.522–1.542 Å range (Fig. S44 and Table 4). While the S_0 optimised geometries contain

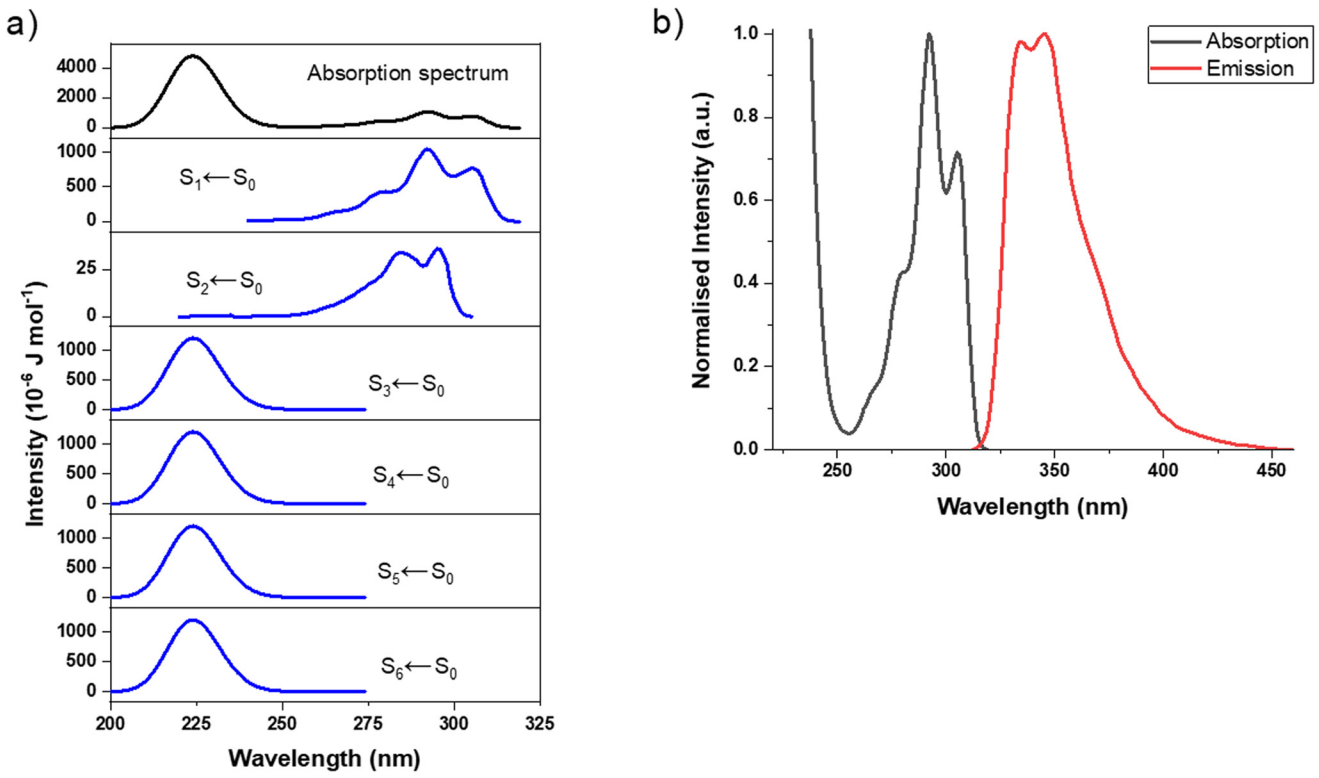

Fig. 8 (a) Calculated absorption spectrum based on combination of vibronic spectra (Adiabatic Hessian) from optimised S_n geometries with cyclohexane as solvent. (b) Simulated absorption and emission spectra for mononaphthyl-*para*-carborane **p1** from vibronic computations.

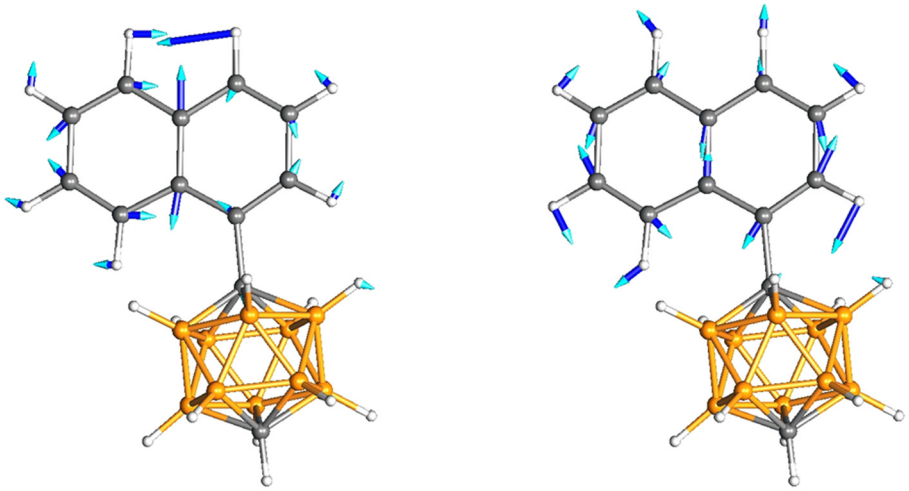

Fig. 9 Vibrations at 1342 cm^{-1} (left) and 1581 cm^{-1} (right) likely to be responsible for the vibronic structure present at 345 nm in the simulated emission of **p1**.

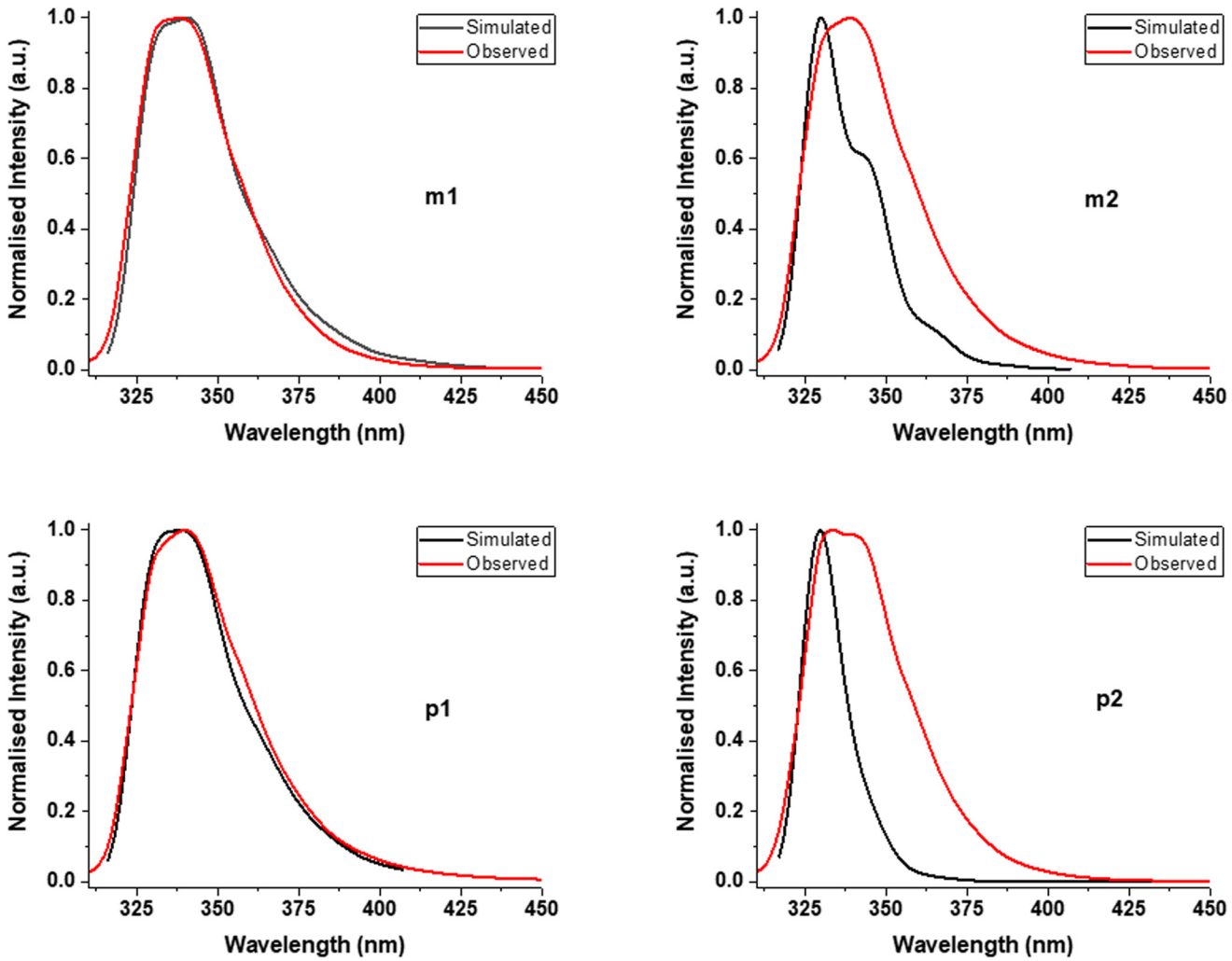

Fig. 10 Comparison between simulated and observed emission spectra with dichloromethane as solvent.

planar naphthyl groups, the observed non-planar naphthyl groups are present due to crystal packing forces (Fig. S43).

The rotation barrier between a phenyl group and the carbon atom of a carborane cluster is negligible (0.2 kcal mol^{-1})[57] whereas the rotation barrier has been estimated to be 10–15 kcal mol^{-1} for a 9-anthacenyl group instead of phenyl.[25,28] Here, the transition state of the mononaphthyl-*para*-carborane located in the C–C rotation is higher than the minimum by 3.3 kcal mol^{-1} (Gibbs free energy 4.0 kcal mol^{-1}) where the hydrogen at C8 is close to the neighbouring hydrogen at boron (Fig. 6). Unlike the 9-anthracenyl group, the 1-naphthyl group is freely rotating in solutions of 1-naphthyl carboranes at ambient temperatures as observed in the sharp solution state NMR peaks here (Fig. S1–S20).

Emissions of interest here involve $S_1 \leftarrow S_0$ transitions thus S_1 excited state geometries for all four compounds were optimised. Interestingly, the naphthyl groups in these geometries are non-planar due to shorter cluster C–naphthyl C bond lengths (Table 4) increasing the steric repulsions between these units. The distortion angles, α and β, used to measure the relative distortions in X-ray structures of anthracenyl carboranes (α = 13.3–14.9°, β = 5.6)[28] reveal essentially similar distortion values (Table 4 and Fig. 6). However, the transition state geometry for the rotation barrier between the naphthyl and carborane units in the excited state geometry of mononaphthyl-*para*-carborane has a planar naphthyl group and a slightly longer cluster C–naphthyl C bond length of 1.507 Å. This geometry is only 3.8 kcal mol^{-1} higher in energy than the excited state minimum.

Absorption spectra of carborane compounds have been predicted by using TD-DFT methods on optimised S_0 geometries for decades. These calculations assume that the geometries of the excited states, S_n (n = 1 or higher), are identical to the optimised S_0 ground state geometry (Vertical Hessian = VH, *e.g.* $S_1' \leftarrow S_0$, Fig. 7). This calculated VH absorption spectrum for mononaphthyl-*para*-carborane (Fig. S45, S46 and Table S7) gives a reasonable overall picture when compared with the observed spectrum but only contains broad bands. It does not show the observed vibronic structure of the low energy bands.

Vibronic calculations provide more realistic absorption spectra as bands with vibronic structure can be modelled. Here, by optimising the S_n (n = 1–6) excited state geometries, each individual vibronic spectrum (Adiabatic Hessian = AH, *e.g.* $S_1 \leftarrow S_0$, Fig. 6) from every $S_n \leftarrow S_0$ transition is combined to generate the simulated absorption spectrum for mononaphthyl-*para*-carborane (Fig. 8).

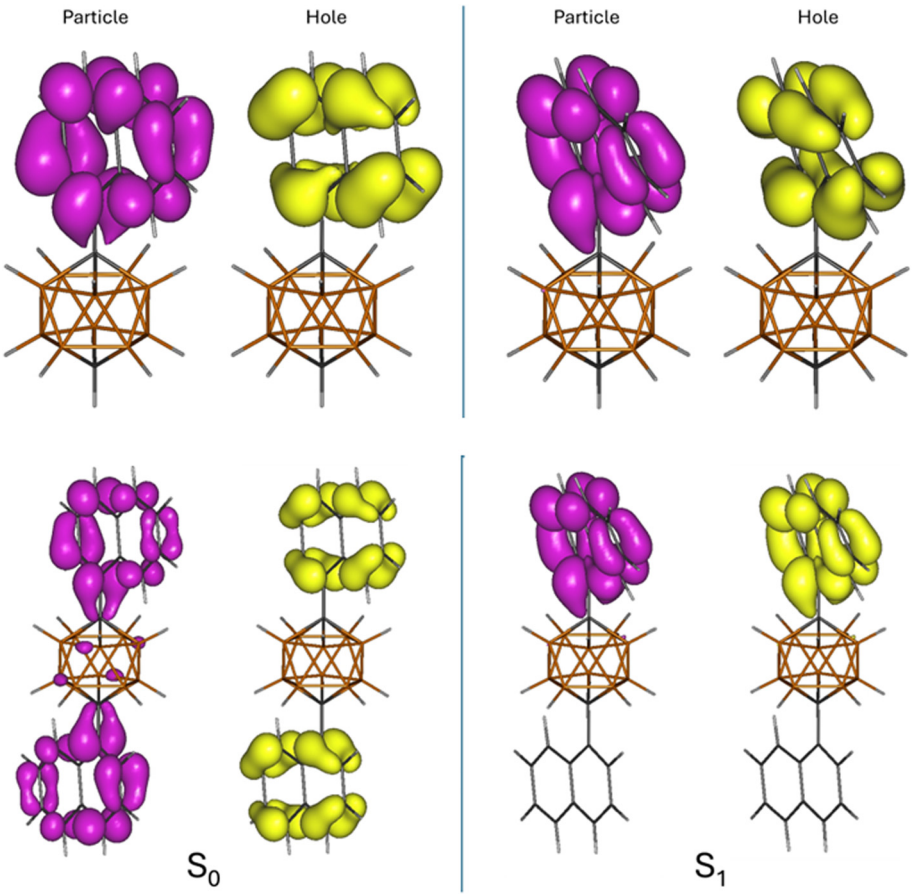

Fig. 11 Natural transition orbitals (NTOs) based on the optimised S_0 and S_1 geometries for **p1** (top) and **p2** (bottom). Purple = particle. Yellow = hole.

Emission data have also been predicted by calculating the $S_1' \leftarrow S_0$ energy using the optimised S_0 geometries (identical to $S_1' \leftarrow S_0$), which can be a good approximation assuming S_0 and S_1 optimised geometries are similar. A more recent and common procedure is determining the $S_1 \leftarrow S_0'$ energy using the optimised S_1 geometry. Again, these TD-DFT methods do not model emission bands with vibronic structures.

The vibronic calculation on the $S_1 \rightarrow S_0$ transition for mononaphthyl-*para*-carborane reveals an emission band with vibronic structure (Fig. 8b and S47) which is in excellent agreement with the observed emission band in cyclohexane (Fig. 5a). Using the energy scaling factor of 0.945 to the calculated energies (as applied for simulated infrared spectra earlier) resulted in excellent agreement of the emission maxima between computed and experimental data. The calculated vibronic bands are predicted to arise from the vibrations of the naphthyl group at 1342 and 1581 cm^{-1} (Fig. 9).

Simulated vibronic emissions were also generated for all four carboranes and compared with observed emissions in dichloromethane solutions (Fig. 10). While the computed and observed mononaphthylcarborane spectra match perfectly, the vibronic bands for the dinaphthylcarborane spectra differ with much lower intensities in the simulated spectra. The nearly identical experimental emission spectra for all compounds infer that the natural transition orbitals (NTOs) involved are located at one naphthyl group.

The orbitals for the optimised S_0 and S_1 states of mononaphthyl-*para*-carborane (Fig. 11) are indeed present at the sole naphthyl group. However, the degenerate NTOs in the S_0 optimised geometry of dinaphthyl-*para*-carborane are located at both naphthyl groups due to symmetry while the NTOs are located at the non-planar naphthyl group in the S_1 geometry. Similar NTOs are present in the *meta*-analogues (Fig. S48). The modelling of the NTOs at the ground state in the dinaphthyl carboranes thus does not model the vibronic calculation correctly. A better model for such disubstituted *meta*- and -*para*-carboranes would be the monosubstituted analogues when predicting their absorption and emission spectra given that the emissions observed are nearly identical.

Conclusions

Naphthalenes with *meta*- and *para*-carboranyl groups are emissive in both solution and solid states with photoluminescence quantum yields of up to 38% and 64% respectively. These emissions have relatively long radiative lifetimes with up to 34 ns in solutions and up to 40 ns in solids. Such yields and lifetimes are unusual in organic luminophores containing carboranes. It is hoped that the field of luminescent *meta*- and *para*-carboranes will be intensively explored in future like the area of so many reported luminescent *ortho*-carboranes in the past decade. Vibronic calculations are demonstrated here to correctly simulate the observed absorption and emission spectra where vibronic structure is observed in some bands. These calculations are expected to support many future photophysical studies of carborane luminophores.

Author contributions

RAH, TDM, JAHM and MAF were responsible for syntheses of the naphthyl carboranes. RAH, LB, AB and MAF carried out the photophysical measurements. MAF was also responsible for the methodology, conceptualisation, characterisation, data analyses, computations, visualisation, writing the original draft, review and editing of the manuscript. DSY determined three crystal structures. MAF supervised RAH, TDM and JAHM and AB supervised LB during their research periods. MAF and AB were in charge of the funding acquisition.

Data availability

Data are provided within the manuscript or supplementary information (SI). Supplementary information containing synthetic details, NMR, MS and IR spectra, further photophysical and computational details and cartesian coordinates of ten optimised geometries is available. See DOI: https://doi.org/10.1039/d5dt02179k.

CCDC 2485369–2485371, 2486934 (**m1**, **m2**, **p1** and **p2**) contain the supplementary crystallographic data for this paper.[58a–d]

Conflicts of interest

There are no conflicts to declare.

Acknowledgements

We thank the Engineering and Physical Sciences Research Council (EPSRC; EP/P505186/1) and the Deutsche Forschungsgemeinschaft (DFG) for financial support. We also thank Dr Toby J. Blundell and Dr Claire Wilson for the X-ray crystallography analysis of compound **p2**.

References

1 L. Weber, J. Kahlert, R. Brockhinke, L. Böhling, A. Brockhinke, H.-G. Stammler, B. Neumann, R. A. Harder and M. A. Fox, *Chem. – Eur. J.*, 2012, **18**, 8347–8357.
2 K.-R. Wee, W.-S. Han, D. W. Cho, S. Kwon, C. Pac and S. O. Kang, *Angew. Chem., Int. Ed.*, 2012, **51**, 2677–2680.
3 R. Núñez, M. Tarrés, A. Ferrer-Ugalde, F. Fabrizi de Biani and F. Teixidor, *Chem. Rev.*, 2016, **116**, 14307–14378.
4 L. Weber, J. Kahlert, L. Böhling, A. Brockhinke, H.-G. Stammler, B. Neumann, R. A. Harder, P. J. Low and M. A. Fox, *Dalton Trans.*, 2013, **42**, 2266–2281.

5 L. Weber, J. Kahlert, R. Brockhinke, L. Böhling, J. Halama, A. Brockhinke, H.-G. Stammler, B. Neumann, C. Nervi, R. A. Harder and M. A. Fox, *Dalton Trans.*, 2013, **42**, 10982–10996.
6 J. Kahlert, L. Böhling, A. Brockhinke, H.-G. Stammler, B. Neumann, L. M. Rendina, P. J. Low, L. Weber and M. A. Fox, *Dalton Trans.*, 2015, **44**, 9766–9781.
7 L. Ji, S. Riese, A. Schmiedel, M. Holzapfel, M. Fest, J. Nitsch, B. F. E. Curchod, A. Friedrich, L. Wu, H. A. Al Mamari, S. Hammer, J. Pflaum, M. A. Fox, D. J. Tozer, M. Finze, C. Lambert and T. B. Marder, *Chem. Sci.*, 2022, **13**, 5205–5219.
8 J. Ochi, K. Tanaka and Y. Chujo, *Angew. Chem., Int. Ed.*, 2020, **59**, 9841–9855.
9 K. Tanaka, M. Gon, S. Ito, J. Ochi and Y. Chujo, *Coord. Chem. Rev.*, 2022, **472**, 214779.
10 K. Tanaka, *Dalton Trans.*, 2024, **53**, 9240–9247.
11 Z. Ran, M. Zhao, J. Shi and L. Ji, *Dyes Pigm.*, 2025, **232**, 112484.
12 S. Kim, D. K. You, N. Kim, I. Shin, D. Kim and K. M. Lee, *Dalton Trans.*, 2025, **54**, 1164–1172.
13 M. Kim, D. K. You, J. Choi, D. Kim and K. M. Lee, *Dyes Pigm.*, 2024, **224**, 11203.
14 K. Kokado and Y. Chujo, *Macromolecules*, 2009, **42**, 1418–1420.
15 K. Kokado and Y. Chujo, *J. Org. Chem.*, 2011, **76**, 316–319.
16 L. Wu, M. Holzapfel, A. Schmiedel, F. Peng, M. Moos, P. Mentzel, J. Shi, T. Neubert, R. Bertermann, M. Finze, M. A. Fox, C. Lambert and L. Ji, *Nat. Commun.*, 2024, **15**, 3005.
17 K.-R. Wee, Y.-J. Cho, J. K. Song and S. O. Kang, *Angew. Chem., Int. Ed.*, 2013, **52**, 9682–9685.
18 H. Naito, K. Nishino, Y. Morisaki, K. Tanaka and Y. Chujo, *Chem. – Asian J.*, 2017, **12**, 2134–2138.
19 S.-Y. Kim, Y.-J. Cho, H.-J. Cho, C. H. Kim and S. O. Kang, *J. Organomet. Chem.*, 2018, **865**, 152–158.
20 S. Yi, M. Kim, C. H. Ryu, D. K. You, Y. J. Seo and K. M. Lee, *Molecules*, 2022, **27**, 6565.
21 Y. J. Seo, M. Kim, D. Kim, N. Kim, I. Shin and K. M. Lee, *Dyes Pigm.*, 2023, **218**, 111451.
22 J. Ochi, T. Yanagihara, K. Tanaka and Y. Chujo, *Phys. Chem. Chem. Phys.*, 2023, **25**, 11839–11844.
23 C. Jia, L. Wang, Y.-N. Ma and Z. Duan, *Organometallics*, 2025, **44**, 938–943.
24 H. Naito, Y. Morisaki and Y. Chujo, *Angew. Chem., Int. Ed.*, 2015, **54**, 5084–5087.
25 H. Naito, K. Nishino, Y. Morisaki, K. Tanaka and Y. Chujo, *Angew. Chem., Int. Ed.*, 2017, **56**, 254–259.
26 H. Naito, K. Uemura, Y. Morisaki, K. Tanaka and Y. Chujo, *Eur. J. Org. Chem.*, 2018, 1885–1890.
27 X. Wu, J. Guo, W. Jia, J. Zhao, D. Jia and H. Shan, *Dyes Pigm.*, 2019, **162**, 855–862.
28 A. V. Marsh, M. J. Dyson, N. J. Cheetham, M. Bidwell, M. Little, A. J. P. White, C. N. Warriner, A. C. Swain, I. McCulloch, P. N. Stavrinou, S. C. J. Meskers and M. Heeney, *Adv. Electron. Mater.*, 2020, **6**, 2000312.
29 J. H. Hong, S. Im, Y. J. Seo, N. Y. Kim, C. H. Lee, M. Kim and K. M. Lee, *J. Mater. Chem. C*, 2021, **9**, 9874–9883.
30 Z. Wang, X. Gou, Q. Shi, K. Liu, X. Chang, G. Wang, W. Xu, S. Lin, T. Liu and Y. Fang, *Angew. Chem., Int. Ed.*, 2022, **61**, e202207619.
31 Y. Ma, X. Wu, Y. Lv, X. Jin, H. Shan and J. Guo, *New J. Chem.*, 2022, **46**, 542–548.
32 M. Kim, S. Yi, D. Kim, I. Shin, Y. J. Seo, D. K. You, C. H. Ryu and K. M. Lee, *Dalton Trans.*, 2023, **52**, 8020–8029.
33 K. Yuhara and K. Tanaka, *Angew. Chem., Int. Ed.*, 2024, **63**, e202319712.
34 K. Kokado, A. Nagai and Y. Chujo, *Tetrahedron Lett.*, 2011, **52**, 293–296.
35 M. Tominaga, H. Naito, Y. Morisaki and Y. Chujo, *New J. Chem.*, 2014, **38**, 5686–5690.
36 M. Tominaga, H. Naito, Y. Morisaki and Y. Chujo, *Asian J. Org. Chem.*, 2014, **3**, 624–631.
37 A. V. Marsh, M. Little, N. J. Cheetham, M. J. Dyson, M. Bidwell, A. J. P. White, C. N. Warriner, A. C. Swain, I. McCulloch, P. N. Stavrinou and M. Heeney, *Chem. – Eur. J.*, 2021, **27**, 1970–1975.
38 J. Ochi, K. Yuhara, K. Tanaka and Y. Chujo, *Chem. – Eur. J.*, 2022, **28**, e202200155.
39 K. Nishino, H. Yamamoto, K. Tanaka and Y. Chujo, *Org. Lett.*, 2016, **18**, 4064–4067.
40 X. Wu, J. Guo, J. Zhao, Y. Che, D. Jia and Y. Chen, *Dyes Pigm.*, 2018, **154**, 44–51.
41 S. Kim, J. H. Lee, H. So, M. Kim, M. S. Mun, H. Hwang, M. H. Park and K. M. Lee, *Inorg. Chem. Front.*, 2020, **7**, 2949–2959.
42 J. Krebs, L. Brändler, I. Krummenacher, A. Friedrich, H. Braunschweig, M. Finze, B. F. E. Curchod and T. B. Marder, *Chem. – Eur. J.*, 2024, **30**, e202401704.
43 S. Nishiyama, J. Ochi and K. Tanaka, *Asian J. Org. Chem.*, 2025, **14**, e202400513.
44 N. Li, X. Wu, Y. Lv, J. Chi and J. Guo, *New J. Chem.*, 2025, **49**, 10530–10537.
45 A. V. Marsh, N. J. Cheetham, M. Little, M. Dyson, A. J. P. White, P. Beavis, C. N. Warriner, A. C. Swain, P. N. Stavrinou and M. Heeney, *Angew. Chem., Int. Ed.*, 2018, **57**, 10640–10645.
46 R. Coult, M. A. Fox, W. R. Gill, P. L. Herbertson, J. A. H. MacBride and K. Wade, *J. Organomet. Chem.*, 1993, **462**, 19–29.
47 M. A. Fox, R. J. Peace, J. A. H. MacBride and K. Wade, *Dalton Trans.*, 1998, 401–411.
48 M. A. Fox, R. Greatrex and A. Nikrahi, *Dalton Trans.*, 2008, 676–684.
49 E. Becerra-Martínez, N. Perez-Hernández, M. Sánchez-Zavala, M. Meléndez-Rodriguez, A. Aristeo-Dominguez, O. R. Suárez-Castillo and P. Joseph-Nathan, *Spectrosc. Lett.*, 2022, **55**, 424–436.
50 M. A. Fox and A. K. Hughes, *Coord. Chem. Rev.*, 2004, **248**, 457–476.

51 S. V. Lindeman, V. E. Shklover, Y. T. Struchkov, I. A. Khotina, T. M. Salykhova, M. M. Teplyakov and V. V. Korshak, *Makromol. Chem.*, 1984, **185**, 417–493.
52 I. B. Berlman, in *Handbook of Fluorescence Spectra of Aromatic Molecules*, Academic Press, New York, 2nd edn, 1971.
53 L. Böhling, A. Brockhinke, J. Kahlert, L. Weber, R. A. Harder, D. S. Yufit, J. A. K. Howard, J. A. H. MacBride and M. A. Fox, *Eur. J. Inorg. Chem.*, 2016, 403–412.
54 J. T. Brownrigg and J. E. Kenny, *J. Phys. Chem. A*, 2009, **113**, 1049–1059.
55 J. B. Aladekomo and J. B. Birks, *Proc. R. Soc. London, Ser. A*, 1965, **284**, 551–565.
56 A. P. Scott and L. Radom, *J. Phys. Chem.*, 1996, **100**, 16502–16513.
57 E. S. Alekseyeva, M. A. Fox, J. A. K. Howard, J. A. H. MacBride and K. Wade, *Appl. Organomet. Chem.*, 2003, **17**, 499–508.
58 (*a*) CCDC 2485369: Experimental Crystal Structure Determination, 2025, DOI: 10.5517/ccdc.csd.cc2pf76l; (*b*) CCDC 2485370: Experimental Crystal Structure Determination, 2025, DOI: 10.5517/ccdc.csd.cc2pf77m; (*c*) CCDC 2485371: Experimental Crystal Structure Determination, 2025, DOI: 10.5517/ccdc.csd.cc2pf78n; (*d*) CCDC 2486934: Experimental Crystal Structure Determination, 2025, DOI: 10.5517/ccdc.csd.cc2pgvpq.